BULLETIN OF THE POLISH ACADEMY OF SCIENCES
TECHNICAL SCIENCES
DOI: 10.24425/bpasts.2026.157323

Optimal collision-free Cartesian trajectory planning for a free-floating space robot with non-zero linear and angular momentum

Tomasz RYBUS

Centrum Badań Kosmicznych Polskiej Akademii Nauk (CBK PAN)

Abstract. An unmanned chaser satellite equipped with a robotic manipulator can be employed for active debris removal and in-orbit servicing missions. It is often assumed that the chaser satellite's control system is switched off during the capture operation performed with the manipulator. However, due to the limited accuracy of the chaser's control system, which relies on thrusters for the approach phase, it may not be possible to obtain zero relative velocity of the chaser with respect to the target satellite. Moreover, in the tangent capture scenario, the chaser satellite is intentionally accelerated to a specific linear velocity before initiating the capture operation. This paper presents an optimal trajectory planning method applicable to a manipulator mounted on a free-floating satellite with non-zero initial velocity and non-zero but constant linear and angular momentum. The trajectory of the manipulator's end-effector is parameterized in the Cartesian space using an 8th-order polynomial. The trajectory planning task is formulated as a constrained nonlinear optimization problem and solved using an interior-point algorithm. Constraints include joint position limits and collision avoidance with spherical obstacles. Two objective functions are considered: minimizing the trajectory length and minimizing the attitude changes of the chaser satellite. The proposed approach is validated through numerical simulations conducted using parameters from a prototype of the 7-DoF WMS 1 Lemur space manipulator. Trajectories obtained with the proposed approach are compared to two non-optimal trajectories: a straight-line trajectory and a collision-free trajectory obtained with the Artificial Potential Field method.

Key words: free-floating manipulator, optimal trajectory planning, obstacle avoidance, space robotics.

1. INTRODUCTION

Due to the potential risk of in-orbit collisions, there is a growing need to capture and remove from orbit defunct satellites and spent rocket stages, known as space debris [1]. One of the approaches considered for conducting active debris removal (ADR) missions involves deploying an unmanned chaser satellite equipped with a robotic manipulator [2, 3]. A gripper attached to the manipulator's end-effector would be used to grasp the uncontrolled target satellite [4]. Such an approach was developed, i.a., for the European Space Agency's e.Deorbit mission, which aimed to demonstrate ADR technologies by capturing and removing the defunct Envisat satellite from orbit [5]. The manipulator-equipped chaser satellite can also be used to prolong operational lifetimes of satellites by performing in-orbit servicing (IOS) [6, 7].

The in-orbit capture operation is the most demanding phase of the proposed ADR and IOS missions. A dynamic coupling exists between the manipulator and the chaser satellite [8]. The chaser may be unable to use its thrusters and reaction wheels to maintain a constant position and orientation relative to the target satellite due to the high and rapidly changing reaction forces and torques induced by the manipulator's motion [9]. Consequently, in all successfully completed demonstration missions involving the grasping of a target satellite using a gripper mounted on a manipulator, such as ETS-VII and Orbital Express, the capture operation was performed without active control of the chaser [10, 11]. In such scenarios, the manipulator-equipped chaser satellite operates in a free-floating mode [12] and is classified as a nonholonomic system [13].

The trajectory planning for the manipulator is typically completed before its motion begins. During manipulator's motion, the closed-loop control system ensures precise tracking of the reference trajectory [14]. In this paper, we focus on the trajectory planning problem. The objective of trajectory planning for in-orbit capture is to generate a feasible path that moves the manipulator from a specified initial configuration to a pose in which the gripper can securely grasp a designated fixture on the target satellite [4]. In the e.Deorbit mission, the selected grasping fixture on the Envisat satellite was its Launch Adapter Ring (LAR) [5]. Ground-based observations show that some pieces of space debris have non-zero angular velocity [15], which makes the trajectory planning task much more difficult, particularly when the object is tumbling [16]. However, due to, among other factors, Earth's gravity gradient and eddy currents induced by the Earth's magnetic field,

*e-mail: trybus@cbk.waw.pl

satellites tend to stabilize [17]. Laser ranging measurements of Envisat show that its angular velocity has systematically decreased in recent years [18]. Moreover, the rotational motion of the target satellite can be effectively slowed down before the start of the capture operation through precisely planned plume impingement using the thrusters of the chaser satellite [19, 20].

Many different methods are proposed for planning the trajectory of a free-floating manipulator, with one of the latest being the algorithm that utilizes the endogenous configuration space approach [21]. Due to the fact that the target satellite usually has complicated shape and is equipped with appendages, the collision avoidance constraints should be considered. The trajectory should ensure no collisions between the manipulator and the elements of the target satellite [22]. Application of well-known collision-free trajectory planning methods, such as the A* algorithm and the Rapidly-exploring Random Trees, is proposed [23–25]. Collision-free trajectory planning methods specifically developed for free-floating manipulators include the Obstacle Vector Field [26]. The use of optimization techniques in trajectory planning is particularly beneficial, as they allow for the achievement of additional goals, such as minimizing changes in the chaser's attitude [27]. However, obstacle avoidance constraints are rarely included in optimal trajectory planning methods applied for free-floating manipulators, although they are considered in [28] and [29].

With a few notable exceptions, such as [30] and [31], optimal trajectory planning methods typically employ trajectory parameterization, treating the parameters that define the trajectory's shape as decision variables. The trajectory may be defined in the configuration space of the manipulator (i.e., the joint space) or in the Cartesian space as the trajectory of the manipulator's end-effector. In the former approach, a parametric function (such as a sine function with a polynomial argument) is selected to represent the position of each joint as a function of time [32–34]. The desired end-effector pose must be stated as a constraint and handled by the optimization algorithm. In the latter approach, a parametric function (such as a Bézier curve or a polynomial) is used to describe each component of the end-effector's configuration as a function of time [27, 35, 36]. Achieving the desired end-effector pose is ensured by appropriate trajectory design. The optimal trajectory planning algorithm seeks parameter values that minimize the objective function while ensuring the fulfillment of constraints, including joint limits and collision avoidance.

It is commonly assumed that no external forces or torques act on the satellite-manipulator system and that the linear and angular momentum of this system are zero. The first assumption is justified, as the influence of the gravity gradient can be neglected over the short timescale of the capture operation due to the small size of the satellite-manipulator system [37]. Consequently, since the chaser satellite is uncontrolled during the capture operation, there are no external forces or torques acting on the system before the gripper makes contact with the target satellite. However, the second assumption is unrealistic. In practice, due to the limited accuracy of the chaser's control system, which relies on thrusters to approach the target satellite, it may not be possible to obtain zero relative velocity of the chaser with respect to the target. The anticipated performance limitations of the chaser's control system during close-proximity operations are discussed in [38] and [39]. Thus, at the beginning of the capture operation, the chaser satellite may have a non-zero initial velocity, and, as a result, non-zero linear and angular momentum. Moreover, in the so-called tangent capture scenario, recently proposed by Seweryn et al. [40], the chaser satellite is intentionally accelerated to a specific linear velocity before initiating the capture operation. As demonstrated in [41], for a tumbling target satellite, tangent capture requires lower control torques in the manipulator's joint and results in lower reaction torques and forces in the gripper compared to a classical scenario, where the chaser has zero initial linear velocity with respect to the target satellite. Furthermore, the tangent capture scenario enhances safety by reducing the risk of collisions during the post-capture phase. Optimal trajectory planning for a free-floating system with non-zero linear and angular momentum is presented in [42], but results are limited to a simplified planar case and no obstacles are considered. To the best of our knowledge, all other papers devoted to the optimal trajectory planning of free-floating manipulators assume that the total linear and angular momentum of the system are zero. Non-zero linear and angular momentum are only considered at the trajectory planning stage for free-flying systems, where the full control of the chaser satellite is assumed during the capture operation [43–45].

In this paper we consider a general three-dimensional satellite-manipulator system with non-zero initial linear and angular velocity, and, consequently, non-zero total linear and angular momentum. The trajectory of the manipulator's end-effector is parametrized in the Cartesian space using 8th-order polynomial. We formulate the trajectory planning task as a constrained nonlinear optimization problem, which is solved with an interior-point algorithm. The constraints include the joint position limits and avoidance of collisions with spherical obstacles. Spheres can be considered as safe zones that surround real obstacles with complex shapes. This simplification reduces the computational complexity involved in collision detection and is suitable for optimization algorithms. We assume that the target satellite is stabilized, or that its angular velocity has been reduced to zero before the beginning of the capture operation, so the obstacles are stationary. The proposed trajectory planning method is validated through numerical simulations using the parameters of a prototype of the WMS 1 Lemur manipulator, a 7 Degrees of Freedom (DoF) robot arm developed for in-orbit capture and servicing operations [46]. The main contribution of this paper lies in abandoning the simplifying assumption of zero linear and angular momentum, and demonstrating the applicability of an optimal trajectory planning method developed without this assumption to a general case of free-floating manipulator operating in the presence of obstacles, which can be avoided through the selection of a high-degree polynomial for trajectory parameterization.

The paper is organized as follows. The dynamic equations of the satellite-manipulator system are derived in Section 2. The optimal trajectory planning method is presented in Section 3.

Section 4 is devoted to validation of the proposed method. The obtained results of numerical simulations, as well as limitations of the proposed method, are discussed in Section 5, while conclusions are given in Section 6.

2. DYNAMICS OF THE SATELLITE-MANIPULATOR SYSTEM

We consider an unmanned chaser satellite equipped with a manipulator that has n rotational joints. The satellite-manipulator system is depicted in Fig. 1. The satellite is not actively controlled during the execution of manipulator motion, so the considered system is free-floating. To derive the dynamic equations of the system, we follow the Generalized Jacobian Matrix (GJM) approach introduced in [47]. The GJM approach was extended by Seweryn and Banaszkiewicz to systems with non-zero and non-conserved linear and angular momentum [31]. The derivation presented herein is based on [48]. The configuration of the satellite-manipulator system is described by the following vector of generalized coordinates:

$$\mathbf{q}_p = [\mathbf{r}_{ch}^T \quad \boldsymbol{\Theta}_{ch}^T \quad \boldsymbol{\theta}_m^T]^T, \tag{1}$$

where $\mathbf{r}_{ch} \in \mathbb{R}^3$ is the position of the chaser satellite center of mass (CoM), $\boldsymbol{\Theta}_{ch} \in \mathbb{R}^3$ is the attitude of the chaser satellite expressed by three Euler angles in ZYX convention, $\boldsymbol{\theta}_m = [\theta_1 \quad \theta_2 \quad \dots \quad \theta_n]^T$, where $\theta_i \in \mathbb{R}^1$ is the angular position of the i-th joint of the manipulator. Unless stated otherwise, vectors are expressed in the inertial frame of reference, denoted by Π_{ine}, which is fixed at an arbitrary point in the Cartesian space.

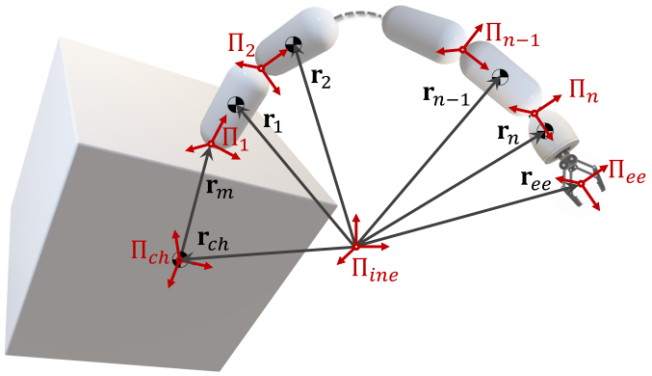

Fig. 1 Diagram of the free-floating satellite-manipulator system.

We chose the following vector of generalized velocities:

$$\mathbf{q}_v = [\mathbf{v}_{ch}^T \quad \boldsymbol{\omega}_{ch}^T \quad \dot{\boldsymbol{\theta}}_m^T]^T, \tag{2}$$

where $\mathbf{v}_{ch} \in \mathbb{R}^3$ and $\boldsymbol{\omega}_{ch} \in \mathbb{R}^3$ denote the linear velocity of the chaser satellite CoM and angular velocity of the chaser satellite, respectively, $\dot{\boldsymbol{\theta}}_m = [\dot{\theta}_1 \quad \dot{\theta}_2 \quad \dots \quad \dot{\theta}_n]^T$, where $\dot{\theta}_i \in \mathbb{R}^1$ is the angular velocity of the i-th joint of the manipulator. The vector of generalized velocities is not a direct time derivative of the vector of generalized coordinates due to the description of three-dimensional rotations of a rigid body (the angular velocity vector's time integral cannot be considered as a representation of the attitude). The following relation holds:

$$\dot{\mathbf{q}}_p = \mathbf{D}\mathbf{q}_v, \tag{3}$$

where $\mathbf{D} \in \mathbb{R}^{(6+n)\times(6+n)}$ is a mapping matrix, defined in [49], that depends on the selected approach to describe rigid body attitude. In such a case, the modified Lagrange equations introduced in [50] must be used to derive the dynamics of the satellite-manipulator system:

$$\frac{d}{dt}\left(\frac{\partial \mathcal{L}}{\partial \mathbf{q}_v}\right) + \mathbf{D}^T(\dot{\mathbf{E}} - \mathbf{H})\frac{\partial \mathcal{L}}{\partial \mathbf{q}_v} - \mathbf{D}^T\frac{\partial \mathcal{L}}{\partial \mathbf{q}_p} = \mathbf{D}^T\mathbf{Q}, \tag{4}$$

where $\mathcal{L}(\mathbf{x}_p, \mathbf{x}_v) \in \mathbb{R}^1$ is the Lagrangian of the system, $\mathbf{E} \in \mathbb{R}^{(6+n)\times(6+n)}$ and $\mathbf{H} \in \mathbb{R}^{(6+n)\times(6+n)}$ are matrices defined in [49] that depend on $\mathbf{q}_v$, while $\mathbf{Q} \in \mathbb{R}^{6+n}$ is the vector of generalized forces:

$$\mathbf{Q} = [\mathbf{F}_{ch}^T \quad \boldsymbol{\tau}_{ch}^T \quad \boldsymbol{\tau}_m^T]^T, \tag{5}$$

where $\mathbf{F}_{ch} \in \mathbb{R}^3$ and $\boldsymbol{\tau}_{ch} \in \mathbb{R}^3$ are the external force and torque acting on the chaser satellite, respectively, $\boldsymbol{\tau}_m = [\tau_1 \quad \tau_2 \quad \dots \quad \tau_n]^T$, where $\tau_i \in \mathbb{R}^1$ is the control torque applied on the i-th joint of the manipulator. We assume $\mathbf{F}_{ch} = \mathbf{0}_{3\times1}$ and $\boldsymbol{\tau}_{ch} = \mathbf{0}_{3\times1}$, but the total linear and angular momentum of the system can be nonzero.

The Lagrangian of the system is given as:

$$\mathcal{L}(\mathbf{x}_p, \mathbf{x}_v) = E_{kin} + E_{pot}, \tag{6}$$

where $E_{kin} \in \mathbb{R}^1$ and $E_{pot} \in \mathbb{R}^1$ are the kinetic and potential energy of the satellite-manipulator system, respectively. In the considered case, the potential energy of this system can be neglected. Thus, $E_{pot} = 0$. The kinetic energy can be expressed as:

$$\begin{aligned} E_{kin} = &\frac{1}{2}(\mathbf{v}_{ch}^T m_{ch}\mathbf{v}_{ch} + \boldsymbol{\omega}_{ch}^T\mathbf{I}_{ch}\boldsymbol{\omega}_{ch}) \\ &+ \frac{1}{2}\left(\sum_{i=1}^{n}\mathbf{v}_i^T m_i\mathbf{v}_i + \sum_{i=1}^{n}\boldsymbol{\omega}_i^T\mathbf{I}_i\boldsymbol{\omega}_i\right), \end{aligned} \tag{7}$$

where $\mathbf{v}_i \in \mathbb{R}^3$ and $\boldsymbol{\omega}_i \in \mathbb{R}^3$ are the linear velocity of the i-th manipulator's link CoM and angular velocity of this link, respectively, $m_{ch} \in \mathbb{R}^1$ and $\mathbf{I}_{ch} \in \mathbb{R}^{3\times3}$ are the mass and mass moment of inertia tensor of the chaser satellite, respectively, while $m_i \in \mathbb{R}^1$ and $\mathbf{I}_i \in \mathbb{R}^{3\times3}$ are the mass and mass moment of inertia tensor of the i-th link, respectively.

The linear velocity of the i-th manipulator's link CoM can be expressed as:

$$\mathbf{v}_i = \mathbf{v}_{ch} + \boldsymbol{\omega}_{ch} \times (\mathbf{r}_i - \mathbf{r}_{ch}) + \mathbf{J}_{t_i}\dot{\boldsymbol{\theta}}_m, \tag{8}$$

where $\mathbf{r}_i \in \mathbb{R}^3$ is the position of the i-th link CoM, while $\mathbf{J}_{t_i} \in \mathbb{R}^{3\times n}$ denotes the translational part of the i-th link's partial Jacobian matrix. Equation (8) can be presented in the following form:

$$\mathbf{v}_i = \mathbf{v}_{ch} + \tilde{\mathbf{r}}_{i\_ch}^T\boldsymbol{\omega}_{ch} + \mathbf{J}_{t_i}\dot{\boldsymbol{\theta}}_m, \tag{9}$$

where $\mathbf{r}_{i\_ch} = \mathbf{r}_i - \mathbf{r}_{ch} \in \mathbb{R}^3$, while $\sim$ denotes a 3×3 skew-symmetric matrix used herein to represent cross products as matrix multiplications. The skew-symmetric matrix of a vector $\mathbf{a} = [a_x \quad a_y \quad a_z]^T$ is defined as follows:

$$\tilde{\mathbf{a}} = \begin{bmatrix} 0 & -a_z & a_y \\ a_z & 0 & -a_x \\ -a_y & a_x & 0 \end{bmatrix}, \tag{10}$$

The angular velocity of the i-th manipulator's link can be expressed as:

$$\boldsymbol{\omega}_i = \boldsymbol{\omega}_{ch} + \mathbf{J}_{r_i}\dot{\boldsymbol{\theta}}_m, \tag{11}$$

where $\mathbf{J}_{r_i} \in \mathbb{R}^{3\times n}$ is the rotational part of the i-th link's partial Jacobian matrix. Partial Jacobians appearing in Eqs. (8), (9) and (11) are partial derivatives of the satellite-manipulator system's direct kinematics with respect to $\mathbf{q}_p$ [51]. They are constructed as though the end-effector is located at the CoM of the i-th link.

By substituting Eqs. (9) and (11) into Eq. (7) and rearranging the resulting expression we obtain the following:

$$E_{kin} = \frac{1}{2}\mathbf{q}_v^T\mathbf{M}\mathbf{q}_v, \tag{12}$$

where $\mathbf{M} \in \mathbb{R}^{(6+n)\times(6+n)}$ is the generalized mass matrix of the satellite-manipulator system defined as:

$$\mathbf{M} = \begin{bmatrix} \mathbf{M}_{v^2} & \mathbf{M}_{v\omega} & \mathbf{M}_{v\dot{\theta}} \\ \mathbf{M}_{v\omega}^T & \mathbf{M}_{\omega^2} & \mathbf{M}_{\omega\dot{\theta}} \\ \mathbf{M}_{v\dot{\theta}}^T & \mathbf{M}_{\omega\dot{\theta}}^T & \mathbf{M}_{\dot{\theta}^2} \end{bmatrix}, \tag{13}$$

where the submatrices $\mathbf{M}_{v^2} \in \mathbb{R}^{3\times3}$, $\mathbf{M}_{v\omega} \in \mathbb{R}^{3\times3}$, and $\mathbf{M}_{\omega^2} \in \mathbb{R}^{3\times3}$ form the mass matrix of the chaser satellite, the submatrices $\mathbf{M}_{v\dot{\theta}} \in \mathbb{R}^{3\times n}$ and $\mathbf{M}_{\omega\dot{\theta}} \in \mathbb{R}^{3\times n}$ form the mass matrix that couples the chaser satellite with the manipulator, while the submatrix $\mathbf{M}_{\dot{\theta}^2} \in \mathbb{R}^{n\times n}$ is the mass matrix of the manipulator. These submatrices are defined as [52]:

$$\mathbf{M}_{v^2} = \left(m_{ch} + \sum_{i=1}^{n} m_i\right)\mathbf{I}_{3\times3}, \tag{14}$$

$$\mathbf{M}_{v\omega} = \sum_{i=1}^{n}\left(m_i\tilde{\mathbf{r}}_{i\_ch}^T\right), \tag{15}$$

$$\mathbf{M}_{\omega^2} = \mathbf{I}_{ch} + \sum_{i=1}^{n}\left(\mathbf{I}_i + m_i\tilde{\mathbf{r}}_{i\_ch}^T\tilde{\mathbf{r}}_{i\_ch}\right), \tag{16}$$

$$\mathbf{M}_{v\dot{\theta}} = \sum_{i=1}^{n}(m_i\mathbf{J}_{ti}), \tag{17}$$

$$\mathbf{M}_{\omega\dot{\theta}} = \sum_{i=1}^{n}\left(\mathbf{I}_i\mathbf{J}_{ri} + m_i\tilde{\mathbf{r}}_{i\_ch}\mathbf{J}_{ti}\right), \tag{18}$$

$$\mathbf{M}_{\dot{\theta}^2} = \sum_{i=1}^{n}(\mathbf{J}_{ri}^T\mathbf{I}_i\mathbf{J}_{ri} + m_i\mathbf{J}_{ti}^T\mathbf{J}_{ti}), \tag{19}$$

where $\mathbf{I}_{3\times3}$ is a 3×3 identity matrix.

By substituting Eq. (12) into Eq. (6), and then by substituting the Lagrangian into Eq. (4), we obtain the dynamic equations of motion of the satellite-manipulator system. These equations can be presented in a compact matrix form:

$$\mathbf{M}\dot{\mathbf{q}}_v + \mathbf{C}\mathbf{q}_v = \mathbf{Q}, \tag{20}$$

where $\mathbf{C} \in \mathbb{R}^{(6+n)\times(6+n)}$ is the Coriolis and centrifugal forces matrix defined as:

$$\mathbf{C} = \dot{\mathbf{M}} + \mathbf{D}^T(\dot{\mathbf{E}} - \mathbf{H})\mathbf{M} - \frac{1}{2}\mathbf{D}^T\left(\frac{\partial(\mathbf{M}\mathbf{q}_v)}{\partial\mathbf{q}_p}\right)^T. \tag{21}$$

The state vector of the satellite-manipulator system, $\mathbf{x} \in \mathbb{R}^{12+2n}$, is introduced as:

$$\mathbf{x} = \begin{bmatrix}\mathbf{q}_p^T & \mathbf{q}_v^T\end{bmatrix}^T. \tag{22}$$

Finally, by utilizing the definition of the state vector provided in Eq. (22) and combining Eqs. (3) and (20), the dynamics of the satellite-manipulator system can be expressed in the state-space form as follows:

$$\dot{\mathbf{x}} = \begin{bmatrix}\dot{\mathbf{q}}_p \\ \dot{\mathbf{q}}_v\end{bmatrix} = \begin{bmatrix}\mathbf{D}\mathbf{q}_v \\ \mathbf{M}^{-1}(\mathbf{Q} - \mathbf{C}\mathbf{q}_v)\end{bmatrix}. \tag{23}$$

The total linear and angular momentum of the satellite-manipulator system can be expressed as:

$$\begin{bmatrix}\mathbf{P} \\ \mathbf{L}\end{bmatrix} = \mathbf{H}_{ch}\begin{bmatrix}\mathbf{v}_{ch} \\ \boldsymbol{\omega}_{ch}\end{bmatrix} + \mathbf{H}_m\dot{\boldsymbol{\theta}}_m = \begin{bmatrix}\mathbf{P}_0 \\ \mathbf{L}_0\end{bmatrix}, \tag{24}$$

where $\mathbf{P}_0 \in \mathbb{R}^3$ and $\mathbf{L}_0 \in \mathbb{R}^3$ are the initial linear and angular momentum of the satellite-manipulator system, respectively, while the matrices $\mathbf{H}_{ch} \in \mathbb{R}^{6\times6}$ and $\mathbf{H}_m \in \mathbb{R}^{6\times n}$ are defined as:

$$\mathbf{H}_{ch} = \begin{bmatrix}\mathbf{M}_{v^2} & \mathbf{M}_{v\omega} \\ \mathbf{M}_{v\omega}^T + \tilde{\mathbf{r}}_{ch}\mathbf{M}_{v^2} & \mathbf{M}_{\omega^2} + \tilde{\mathbf{r}}_{ch}\mathbf{M}_{v\omega}\end{bmatrix}, \tag{25}$$

$$\mathbf{H}_m = \begin{bmatrix}\mathbf{M}_{v\dot{\theta}} \\ \mathbf{M}_{\omega\dot{\theta}} + \tilde{\mathbf{r}}_{ch}\mathbf{M}_{v\dot{\theta}}\end{bmatrix}. \tag{26}$$

Note that, in contrast to e.g. [25], [26], and [53] we do not assume that the total linear and angular momentum of the system are zero. Thus, $\mathbf{P}_0 \neq \mathbf{0}$ and $\mathbf{L}_0 \neq \mathbf{0}$. Consequently, we can perform the trajectory planning for systems with non-zero initial linear and angular velocities of the chaser satellite.

Equation (24) can be transformed to express the relation between the angular velocities of manipulator's joints and the linear and angular velocity of the chaser:

$$\begin{bmatrix}\mathbf{v}_{ch} \\ \boldsymbol{\omega}_{ch}\end{bmatrix} = \mathbf{H}_{ch}^{-1}\left(\begin{bmatrix}\mathbf{P}_0 \\ \mathbf{L}_0\end{bmatrix} - \mathbf{H}_m\dot{\boldsymbol{\theta}}_m\right), \tag{27}$$

The forward kinematics of the satellite-manipulator system on the velocity level is given as follows:

$$\begin{bmatrix}\mathbf{v}_{ee} \\ \boldsymbol{\omega}_{ee}\end{bmatrix} = \mathbf{J}_{ch}\begin{bmatrix}\mathbf{v}_{ch} \\ \boldsymbol{\omega}_{ch}\end{bmatrix} + \mathbf{J}_m\dot{\boldsymbol{\theta}}_m, \tag{28}$$

where $\mathbf{v}_{ee} \in \mathbb{R}^3$ and $\boldsymbol{\omega}_{ee} \in \mathbb{R}^3$ are the linear and angular velocity of the end-effector, respectively, $\mathbf{J}_m \in \mathbb{R}^{6\times n}$ is the standard kinematic Jacobian of a fixed-base manipulator, while $\mathbf{J}_{ch} \in \mathbb{R}^{6\times6}$ is the Jacobian of the chaser satellite defined as follows:

$$\mathbf{J}_{ch} = \begin{bmatrix}\mathbf{I}_{3\times3} & \tilde{\mathbf{r}}_{ee\_ch}^T \\ \mathbf{0}_{3\times3} & \mathbf{I}_{3\times3}\end{bmatrix}, \tag{29}$$

where $\mathbf{0}_{3\times3}$ is a 3×3 matrix filled with zeros, while $\mathbf{r}_{ee\_ch} = \mathbf{r}_{ee} - \mathbf{r}_{ch} \in \mathbb{R}^3$, and $\mathbf{r}_{ee} \in \mathbb{R}^3$ is the position of the manipulator's end-effector.

Substituting Eq. (27) into Eq. (28) yields:

$$\begin{bmatrix}\mathbf{v}_{ee} \\ \boldsymbol{\omega}_{ee}\end{bmatrix} = \mathbf{J}_{ch}\mathbf{H}_{ch}^{-1}\begin{bmatrix}\mathbf{P}_0 \\ \mathbf{L}_0\end{bmatrix} + (\mathbf{J}_m - \mathbf{J}_{ch}\mathbf{H}_{ch}^{-1}\mathbf{H}_m)\dot{\boldsymbol{\theta}}_m. \tag{30}$$

Finally, from Eq. (30) we obtain the following relation between the end-effector's velocity and velocities of manipulator's joints:

$$\dot{\boldsymbol{\theta}}_m = \mathbf{J}_D^{\#}\left(\begin{bmatrix}\mathbf{v}_{ee} \\ \boldsymbol{\omega}_{ee}\end{bmatrix} - \mathbf{J}_{ch}\mathbf{H}_{ch}^{-1}\begin{bmatrix}\mathbf{P}_0 \\ \mathbf{L}_0\end{bmatrix}\right), \tag{31}$$

where $\mathbf{J}_D \in \mathbb{R}^{6\times n}$ is the GJM matrix also known as the Dynamic Jacobian of free-floating space manipulator [54] defined as:

$$\mathbf{J}_D = \mathbf{J}_m - \mathbf{J}_{ch}\mathbf{H}_{ch}^{-1}\mathbf{H}_m, \tag{32}$$

while # denotes the Moore-Penrose pseudoinverse of a matrix [55], which must be used here because for a redundant manipulator $\mathbf{J}_D$ is a non-square matrix. For a redundant manipulator in a given configuration, there are infinitely many ways to assign joint velocities that achieve the required linear and angular velocity of the end-effector. The Moore-Penrose pseudoinverse of a given matrix is unique and in the considered case allows us to select the solution that ensures the smallest Euclidean norm of joint velocities. Due to the fact that $\mathbf{J}_D$ depends on the mass and inertia parameters of the satellite-manipulator system, the free-floating manipulator exhibits dynamic singularities, the location of which cannot be determined from the manipulator's kinematic structure alone [56]. Equation (31) is applicable only in configurations free of dynamic singularities. As the problem of singularity avoidance is outside the scope of this paper, we only consider scenarios, in which the manipulator operates sufficiently far from singular configurations.

3. OPTIMAL TRAJECTORY PLANNING METHOD

The task of the optimal trajectory planning method is to find an optimal collision-free trajectory from the specified initial configuration and velocity of the manipulator to the desired position, orientation, linear velocity, and angular velocity of the end-effector, while taking into account joint position limits and specified non-zero initial linear and angular velocity of the chaser satellite. The trajectory is defined by a set of parameters that form the vector of decision variables, whose values, ensuring the minimization of the selected objective function, are determined during the process of solving the optimization problem.

3.1. Trajectory parametrization.

In [57] a simple polynomial function is used to define the angular position of each joint of the manipulator as a function of time. We adapt such a parameterization to define the components of the end-effector's pose as a function of time. The end-effector pose has six components: three components of the end-effector position, $\mathbf{r}_{ee}$, and three components of the end-effector orientation expressed as Euler angles in ZYX convention, $\boldsymbol{\Theta}_{ee} \in \mathbb{R}^3$. The end-effector trajectory in the Cartesian space is defined as: $\mathbf{p}_{ee}(t) = [\mathbf{r}_{ee}^T(t) \quad \boldsymbol{\Theta}_{ee}^T(t)]^T$. Each component of this trajectory, denoted as p_k for $k = 1, 2, \ldots, 6$, is described by a polynomial function of time. While in [57] a 7th-order polynomial is used, we use an 8th-order polynomial to allow more freedom in selection of the trajectory shape. Preliminary investigations showed that 8th-order is sufficient for the considered problem, while using a polynomial of even higher order would unnecessarily increase the number of free coefficients that form the vector of decision variables, increasing the time required to solve the optimization problem. The k-th component of the trajectory is given as:

$$\begin{aligned} p_k = a_{8,k}t^8 + a_{7,k}t^7 + a_{6,k}t^6 + a_{5,k}t^5 + a_{4,k}t^4 \\ + a_{3,k}t^3 + a_{2,k}t^2 + a_{1,k}t + a_{0,k}, \end{aligned} \tag{33}$$

where $a_{0,k} \in \mathbb{R}^1$, $a_{1,k} \in \mathbb{R}^1$, …, $a_{8,k} \in \mathbb{R}^1$ are the constant coefficients of the polynomial. Differentiating Eq. (33) with respect to time yields the end-effector trajectory on the velocity level:

$$\begin{aligned} \dot{p}_k = 8a_{8,k}t^7 + 7a_{7,k}t^6 + 6a_{6,k}t^5 + 5a_{5,k}t^4 \\ +4a_{4,k}t^3 + 3a_{3,k}t^2 + 2a_{2,k}t + a_{1,k}. \end{aligned} \tag{34}$$

Note that for $k \in \{4,5,6\}$ we get time derivatives of the Euler angles. Thus, to obtain $\mathbf{w}_{ee}(t) = [\mathbf{v}_{ee}^T(t) \quad \boldsymbol{\omega}_{ee}^T(t)]^T$ from $\dot{\mathbf{p}}_{ee}(t) = [\mathbf{v}_{ee}^T(t) \quad \dot{\boldsymbol{\Theta}}_{ee}^T(t)]^T$ we need to use a proper mapping matrix, as in Eq. (3).

By differentiating Eq. (34) with respect to time we obtain the trajectory on the acceleration level:

$$\begin{aligned} \ddot{p}_k = 56a_{8,k}t^6 + 42a_{7,k}t^5 + 30a_{6,k}t^4 + 20a_{5,k}t^3 \\ + 12a_{4,k}t^2 + 6a_{3,k}t + 2a_{2,k}. \end{aligned} \tag{35}$$

In the considered scenario of in-orbit capture maneuver, the start and end points of the end-effector's trajectory are precisely defined, as the initial configuration of the end-effector relative to the target satellite and the location of the grasping point are known prior to trajectory planning. For each component of the trajectory, the initial position, velocity, and acceleration are specified, along with the desired final position, velocity, and acceleration: $p_k(t_0) = p_{k_0}$, $\dot{p}_k(t_0) = \dot{p}_{k_0}$, $\ddot{p}_k(t_0) = \ddot{p}_{k_0}$, $p_k(t_f) = p_{k_f}$, $\dot{p}_k(t_f) = \dot{p}_{k_f}$, $\ddot{p}_k(t_f) = \ddot{p}_{k_f}$, where t_0 is the specified initial time, while t_f is the specified time at which the end-effector should reach the end point of the trajectory.

For each component of the end-effector trajectory, nine unknown coefficients of the polynomial appear in Eqs. (33) – (35). Considering the six conditions arising from the defined start and end points of the trajectory, three coefficients remain free, enabling us to shape the trajectory. We choose coefficients associated with the terms that have the highest order of t, namely $a_{6,k}$, $a_{7,k}$, and $a_{8,k}$, as free coefficients that will form the vector of decision variables. The remaining coefficients are given by the following expressions resulting from the aforementioned conditions:

$$a_{0,k} = p_{k_0}, \tag{36}$$

$$a_{1,k} = \dot{p}_{k_0}, \tag{37}$$

$$a_{2,k} = \ddot{p}_{k_0}, \tag{38}$$

$$\begin{aligned} a_{3,k} = \frac{1}{2t_f^3}\big(-20p_{k_0} + 20p_{k_f} - 12\dot{p}_{k_0}t_f - 8\dot{p}_{k_f}t_f \\ -3\ddot{p}_{k_0}t_f^2 + \ddot{p}_{k_f}t_f^2 - 12a_{8,k}t_f^8 - 6a_{7,k}t_f^7 - 2a_{6,k}t_f^6\big), \end{aligned} \tag{39}$$

$$\begin{aligned} a_{4,k} = \frac{1}{2t_f^4}\big(30p_{k_0} - 30p_{k_f} + 16\dot{p}_{k_0}t_f + 14\dot{p}_{k_f}t_f \\ +3\ddot{p}_{k_0}t_f^2 - 2\ddot{p}_{k_f}t_f^2 + 30a_{8,k}t_f^8 + 16a_{7,k}t_f^7 + 6a_{6,k}t_f^6\big), \end{aligned} \tag{40}$$

$$\begin{aligned} a_{5,k} = \frac{1}{2t_f^5}\big(-12p_{k_0} + 12p_{k_f} - 6\dot{p}_{k_0}t_f - 6\dot{p}_{k_f}t_f \\ -\ddot{p}_{k_0}t_f^2 + \ddot{p}_{k_f}t_f^2 - 20a_{8,k}t_f^8 - 12a_{7,k}t_f^7 - 6a_{6,k}t_f^6\big). \end{aligned} \tag{41}$$

3.2. Optimal trajectory planning problem.

The trajectory planning task is formulated as an optimization problem, in which the vector of decision variables $\boldsymbol{\xi} \in \mathbb{R}^{18}$ is defined as follows:

$$\boldsymbol{\xi} = [a_{6,1} \quad a_{7,1} \quad a_{8,1} \quad \dots \quad a_{6,6} \quad a_{7,6} \quad a_{8,6}]^T. \tag{42}$$

Note that the size of $\boldsymbol{\xi}$ results from the selected trajectory parametrization and the order of the polynomial in Eq. (33). A given value of $\boldsymbol{\xi}$ uniquely determines the trajectory of the end-effector in the Cartesian space, $\mathbf{p}_{ee}(t)$, for which, with the use of Eq. (31), we obtain the trajectory of the manipulator in the joint space on the velocity level, $\dot{\boldsymbol{\theta}}_m(t)$. Then, the 4th-order Runge-Kutta (RK-IV) method is employed to numerically solve the dynamic equations of motion, given in the state-space form as Eq. (23), while Eq. (27) is used to determine the linear and angular velocity of the chaser satellite. The step size of the RK-IV method is defined as $\Delta t = t_f/(n_p - 1)$, where $n_p \in \mathbb{R}^1$ is the number of points comprising the trajectory. As explained in the Introduction, the necessity of using dynamics equations at the trajectory planning stage is a major difference between trajectory planning for fixed-base manipulators operating on Earth and free-floating manipulators operating in orbit.

The objective of the optimization problem is to minimize a multivariable function $J(\boldsymbol{\xi})$: $\mathbb{R}^{18} \rightarrow \mathbb{R}^1$, subject to specified equality and inequality constraints:

$$\min_{\boldsymbol{\xi}} J(\boldsymbol{\xi}) \quad \text{s.t.} \begin{cases} R_{obst}(\boldsymbol{\xi}) = 0 \\ \max \theta_i(\boldsymbol{\xi}) - \theta_{i\_max} \leq 0, \text{for } i = 1, 2, \dots, n \\ -\min \theta_i(\boldsymbol{\xi}) + \theta_{i\_min} \leq 0, \text{for } i = 1, 2, \dots, n \end{cases}, \tag{43}$$

where $R_{obst}(\boldsymbol{\xi}) \in \mathbb{R}^1$ represents the penalty function that enforces the obstacle avoidance condition, while $\max \theta_i(\boldsymbol{\xi})$ and $\min \theta_i(\boldsymbol{\xi})$ are the maximal and the minimal values of the i-th joint angular position, respectively, determined from $\theta_i(t)$, which results from the given $\boldsymbol{\xi}$. The optimization problem defined in Eq. (43) is solved with an interior-point algorithm.

Two variants of $J(\boldsymbol{\xi})$ are considered: one that minimizes the trajectory length in the manipulator's joint space and another that minimizes the maximum value of Euler angles describing the satellite's attitude. The former approach, based on [29], allows obtaining the shortest possible trajectory, which should be the most feasible for practical implementation, while the latter approach aims at minimizing attitude changes caused by the manipulator's motion and the initial angular velocity of the chaser satellite. These variants are defined as:

$$J_L = \int_{t_0}^{t_f} \sqrt{\sum\nolimits_{i=1}^{n} \left(\frac{d\theta_i(t)}{dt}\right)^2}\, dt, \tag{44}$$

$$J_\Theta = \max(\max(|\psi_{ch}(t)|), \max(|\theta_{ch}(t)|), \max(|\varphi_{ch}(t)|)), \tag{45}$$

where $\psi_{ch} \in \mathbb{R}^1$, $\theta_{ch} \in \mathbb{R}^1$, and $\varphi_{ch} \in \mathbb{R}^1$ are the Euler angles that describe the chaser's attitude: $\boldsymbol{\Theta}_{ch} = [\psi_{ch} \quad \theta_{ch} \quad \varphi_{ch}]^T$. The integral in Eq. (44) is calculated numerically using the rectangle method.

3.3. Obstacle avoidance penalty function.

For the purpose of collision-free trajectory planning in the field of space robotics it is common to assume very simple shapes of obstacles [22]. Real obstacles with complex shapes are contained within simple primitives. In [29, 43, 58] obstacles are modeled as spheres. We adopt the same approach in our study.

The number of obstacles is represented by $n_\Gamma \in \mathbb{R}^1$. The k-th obstacle is defined by its radius, $\rho_{\Gamma_k} \in \mathbb{R}^1$, and the position of its center, $\mathbf{r}_{\Gamma_k} \in \mathbb{R}^3$. The obstacle avoidance penalty function in Eq. (43) has the following form:

$$R_{obst}(\boldsymbol{\xi}) = \sum_{k=1}^{n_\Gamma} \sum_{i=1}^{n_p} V_{ki}, \tag{46}$$

where the indices i and k refer to the i-th point on the trajectory and k-th obstacle, respectively, while $V_{ki} \in \mathbb{R}^1$ is given as [29]:

$$V_{ki} = \begin{cases} 0, & if\ \delta_k \geq \rho_{\Gamma_k} \\ g_1(\rho_{\Gamma_k} - \delta_k)^{g_2}, & if\ \delta_k < \rho_{\Gamma_k} \end{cases}, \tag{47}$$

where $g_1 \in \mathbb{R}^1$ and $g_2 \in \mathbb{R}^1$ are constant parameters that determine how the penalty scales with the depth of the link's intrusion into the obstacle, while $\delta_k \in \mathbb{R}^1$ is the shortest distance between the manipulator and the center of the k-th obstacle calculated using simple analytical expressions for the distance between a line segment and a point, where the line segments under consideration are the lines connecting consecutive manipulator joints. The function $R_{obst}(\boldsymbol{\xi})$ in Eq. (43) guarantees that the lines connecting the manipulator joints remain outside of spherical obstacles, since the constraint $R_{obst}(\boldsymbol{\xi}) = 0$ is satisfied only if, for every point on the trajectory, the shortest distance δ_k is not less than the radius of the k-th obstacle. To account for the diameter of manipulator's link, the radius of the sphere must be sufficiently larger so that a certain distance, at least as large as the radius of the thickest link, remains between the surface of the sphere and the actual obstacle inside it.

4. VALIDATION OF THE PROPOSED METHOD

The optimal collision-free trajectory planning method described in Section 3 was implemented in Matlab R2015a and integrated with the 'Simulation tool for space robotics,' an in-house software developed at the Space Research Centre of the Polish Academy of Sciences for performing dynamic simulations of satellite-manipulator system [59].

4.1. Selection of reference and optimal trajectories for comparison.

Two variants of the proposed approach are evaluated: one based on the objective function defined in Eq. (44) which minimizes the trajectory length and another based on the objective function defined in Eq. (45) which minimizes the maximum value of Euler angles describing the satellite's attitude. Subsequently, the trajectory obtained with the first variant will be denoted as $\min(\mathrm{L})$, and that obtained with the second variant as $\min(\Theta_{\max})$. These two trajectories are compared with two non-optimal trajectories. The first one is obtained using the same parametrization, but with free coefficients equal to zero, i.e., $a_{6,k} = a_{7,k} = a_{8,k} = 0$, resulting in a straight-line path. This

trajectory can be considered as the simplest approach that not only does not take into account any optimization but also does not take into account obstacles.

The second non-optimal trajectory is obtained using a simple variant of the Artificial Potential Field (APF) method [60]. The APF method is widely employed for collision-free trajectory planning of robots operating on Earth [61], whereas [62] proposed its application to a free-floating manipulator. In this approach, the manipulator moves under the influence of an artificial force field. The end-effector is attracted toward the desired final pose, while obstacles exert repulsive forces on the manipulator's links. In our implementation of the APF method, the attractive force has a constant magnitude, whereas the repulsive force is proportional to the distance between the manipulator and the obstacle (specifically, to determine the value of the repulsive potential, we use the Born approximation of the Yukawa potential). To make a fair comparison with the optimal trajectory planning method proposed in our paper, we use the APF method to generate the reference end-effector trajectory in the Cartesian space, rather than directly obtaining the manipulator trajectory in the joint space, as, e.g., in [62]. The motion of the joints results from Eq. (31), in which the Moore-Penrose pseudoinverse of the Dynamic Jacobian matrix is used.

4.2. Parameters of the satellite-manipulator system.

We assume that the chaser satellite, equipped with the manipulator, belongs to the class of small satellites and has a total mass of $m_{ch} = 350$ kg at the start of the capture operation. Its moments of inertia around the axes of Π_{ch} located in the chaser's CoM are: $I_{xx} = 19.7$ kg/m^2, $I_{yy} = 15.7$ kg/m^2, and $I_{zz} = 26.9$ kg/m^2, while all products of inertia are zero. The manipulator mounting point, i.e., the position of the first joint with respect to the origin of Π_{ch}, is: $\mathbf{r}_m^{(\Pi_{ch})} = [0.2\text{ m} \quad 0.1\text{ m} \quad 0.4\text{ m}]^T$, where the superscript indicates that this vector is expressed in Π_{ch}. The kinematics, mass and geometrical properties of the manipulator used in numerical simulations are based on the parameters of the prototype of the WMS 1 Lemur manipulator [46, 63]. The total mass of the manipulator, including gripper, is 25.9 kg, while its total length in the fully stretched configuration is 3.2 m.

4.3. Simulation scenario.

We take the origin of Π_{ine} to be located at the initial position of the chaser's CoM, and we set the orientation of Π_{ine} to be aligned with that of Π_{ch}. As a result, $\mathbf{r}_{ch}(t_0) = \mathbf{0}_{3\times1}$ and $\boldsymbol{\Theta}_{ch}(t_0) = \mathbf{0}_{3\times1}$, where $t_0 = 0$. We assume that the chaser satellite has non-zero initial velocity, resulting either from inaccuracy of its control system during the approach to the target satellite or from intentional setting for the tangent capture maneuver. The initial linear velocity of the chaser satellite at the beginning of the capture phase, i.e., after the manipulator's deployment, is: $\mathbf{v}_{ch}(t_0) = [0.02\text{ m/s} \quad 0 \quad 0.05\text{ m/s}]^T$, while the initial angular velocity is: $\boldsymbol{\omega}_{ch}(t_0) = [0 \quad 2.865\text{ deg/s} \quad 0.573\text{ deg/s}]^T$.

The initial configuration of the manipulator, reached after the manipulator's deployment, is defined by the following positions of manipulator joints: $\theta_1(t_0) = 12.54$ deg, $\theta_2(t_0) = -13.91$ deg, $\theta_3(t_0) = 0$ deg, $\theta_4(t_0) = -64.93$ deg, $\theta_5(t_0) = -105.28$ deg, $\theta_6(t_0 0) = 65.61$ deg, and $\theta_7(t_0) = -127.95$ deg. In the WMS 1 Lemur manipulator, the third joint is treated as the one that introduces redundancy. For the purpose of solving the inverse kinematics problem using analytical methods, the position of this joint is set to zero. The initial position and orientation of the end-effector is: $\mathbf{r}_{ee}(t_0) = [0.8\text{ m} \quad 0.4\text{ m} \quad 0.6\text{ m}]^T$ and $\boldsymbol{\Theta}_{ee}(t_0) = [-45\text{ deg} \quad 55\text{ deg} \quad -65\text{ deg}]^T$. We assume that the manipulator's trajectory in the deployment phase was planned in such a way, that the linear and angular velocity of the end-effector with respect to Π_{ine} are zero at the beginning of the considered maneuver: $\mathbf{v}_{ee}(t_0) = \mathbf{0}_{3\times1}$ and $\boldsymbol{\omega}_{ee}(t_0) = \mathbf{0}_{3\times1}$. However, the presented approach is applicable for any initial velocity of the end-effector. From the solution of the inverse kinematics problem at the velocity level we obtain the following initial angular velocities of the manipulator's joints: $\dot{\theta}_1(t_0) = 0.261$ deg/s, $\dot{\theta}_2(t_0) = -0.076$ deg/s, $\dot{\theta}_3(t_0) = -0.071$ deg/s, $\dot{\theta}_4(t_0) = -1.794$ deg/s, $\dot{\theta}_5(t_0) = -5.066$ deg/s, $\dot{\theta}_6(t_0) = -0.416$ deg/s, and $\dot{\theta}_7(t_0) = -0.969$ deg/s.

The goal of the trajectory planning task is to move the end-effector from the given initial pose to the desired final pose specified as: $\mathbf{p}_{ee}(t_f) = [\mathbf{r}_{ee}^T(t_f) \quad \boldsymbol{\Theta}_{ee}^T(t_f)]^T$, where $\mathbf{r}_{ee}(t_f) = [1.7\text{ m} \quad 0.4\text{ m} \quad 0.6\text{ m}]^T$, while $\boldsymbol{\Theta}_{ee}(t_f) = [-65\text{ deg} \quad 80\text{ deg} \quad -85\text{ deg}]^T$. The final pose should be reached at $t_f = 10$ s. The desired final linear and angular velocity of the end-effector with respect to Π_{ine} is: $\mathbf{v}_{ee}(t_f) = \mathbf{0}_{3\times1}$ and $\boldsymbol{\omega}_{ee}(t_f) = \mathbf{0}_{3\times1}$ There are three obstacles in the manipulator workspace. We assume that these obstacles are elements of the target satellite, so they are stationary in Π_{ine} since the target satellite is also stationary. As explained in Section 3.3, obstacles of complex shapes are contained within spheres, the radius of which is sufficiently larger to account for the diameter of the manipulator links. The centers of spheres are located at the following positions: $\mathbf{r}_{\Gamma_1} = [1.2\text{ m} \quad 0.4\text{ m} \quad 0.54\text{ m}]^T$, $\mathbf{r}_{\Gamma_2} = [1.2\text{ m} \quad 0.7\text{ m} \quad 0.7\text{ m}]^T$, $\mathbf{r}_{\Gamma_3} = [1.2\text{ m} \quad 0.4\text{ m} \quad 0.54\text{ m}]^T$. They have the following radii: $\rho_{\Gamma_1} = 0.2$ m, $\rho_{\Gamma_2} = 0.15$ m, and $\rho_{\Gamma_3} = 0.25$ m.

4.4. Results of numerical simulations.

The trajectory planning was performed with the following values of constant parameters: $g_1 = 2.5$, $g_2 = 1$. The value of g_2 was chosen to be the same as in one of the two cases considered in [29]. For this value, the penalty for violating the obstacle avoidance condition is linearly proportional to the depth of the link's intrusion into the obstacle, which may be considered a natural first choice [64]. The value of g_1 was chosen so that, for the selected solver tolerance, even a very small collision produces a penalty large enough to violate the collision avoidance constraint. The selected values allow for finding a solution in various scenarios, although some scenarios may require selecting different values. The interior-point algorithm used to solve the optimization problem was initialized with the following value of the vector of decision

variables: $\boldsymbol{\xi} = \mathbf{0}_{18\times1}$. The trajectory is composed of $n_p = 50$ points. After the trajectory planning stage, the control torques for manipulator joints were calculated from Eq. (20), and an open-loop simulation was performed in Simulink environment using a SimMechanics model of the satellite-manipulator system.

Frames from an animation depicting the satellite-manipulator system during the execution of the manipulator's optimal minimal-length trajectory are provided in Fig. 2. The position and orientation of the manipulator's end-effector are presented in Fig. 3, while the position and attitude of the chaser satellite are shown in Fig. 4. Figure 5 presents the linear and angular velocity of the satellite. Finally, the distance between the surface of an obstacle closest to the manipulator and center line of manipulator's links is depicted in Fig. 6. On all plots 'Straight-line' refers to the straight-line trajectory, 'APF' refers to the trajectory planned with the APF method, while min(L) and $\min(\Theta_{\max})$ refer to optimal trajectories planned with the objective function defined in Eqs. (44) and (45), respectively.

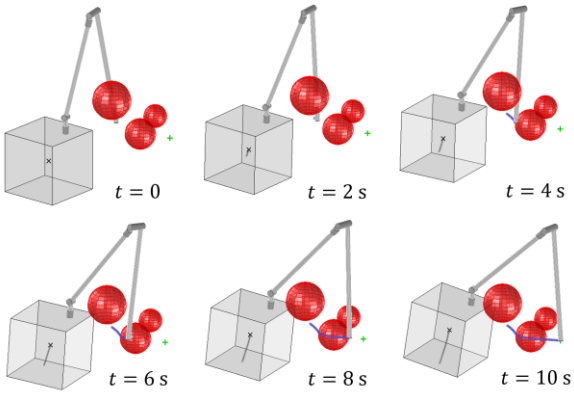

Fig. 2 Frames from an animation depicting the satellite-manipulator system during the execution of the manipulator's optimal minimal-length trajectory. Obstacles are shown as red spheres. The trajectory of the end-effector is marked with a blue line, while the trajectory of the chaser satellite CoM is marked with a gray line.

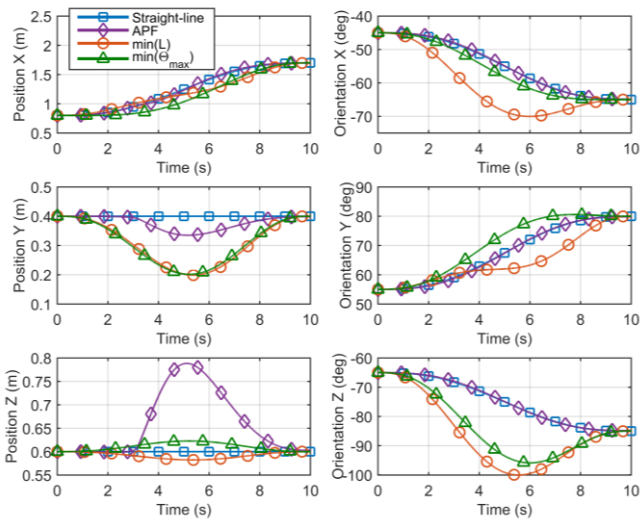

Fig. 3 Position and orientation of the manipulator's end-effector.

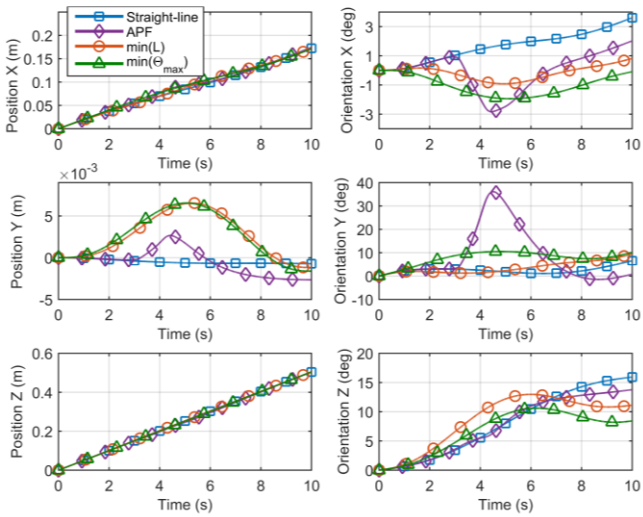

Fig. 4 Position and attitude of the chaser satellite.

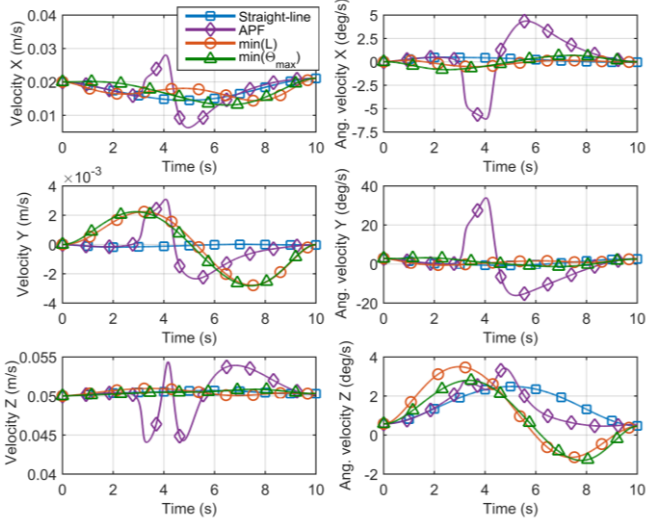

Fig. 5 Linear and angular velocity of the chaser satellite.

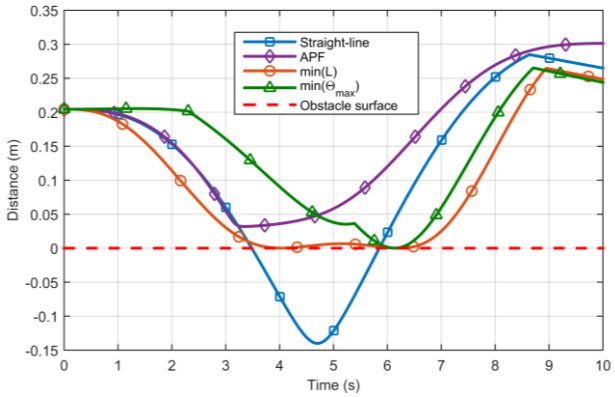

Fig. 6 Distance between the obstacle closest to the manipulator and center line of manipulator's links.

5. DISCUSSION

5.1. Analysis of obtained results.

In the considered scenario, the proposed method was able to find the solution to the optimization problem for both the minimal-length trajectory (min(L)) and the trajectory that minimizes the maximum value of the Euler angles describing the satellite's attitude ($\min(\Theta_{\max})$). The adopted trajectory parameterization ensures that the end-effector reaches the desired pose. The zero initial and final end-effector linear and angular velocities imposed in the considered scenario result in non-zero initial and final velocities of the manipulator's joints. The accuracy obtained in numerical simulations for the considered scenario depends only on the solver settings and the step size. While equations presented in Sections 2 and 3 are used in the trajectory planning stage, the open-loop simulation performed using the SimMechanics model allows for independent verification of the correctness of both the mathematical model and the planning algorithm.

Two optimal trajectories were compared with two non-optimal trajectories: a straight-line trajectory and collision-free trajectory planned with the APF method. The obtained length of the $\min(\mathrm{L})$ trajectory is 2.65% shorter than that of the non-optimal straight-line trajectory. Here we consider the length of a trajectory in the joint space, not the Cartesian space, and a straight end-effector trajectory in the Cartesian space does not turn out to be the shortest trajectory in the joint space. The length of the $\min(\mathrm{L})$ trajectory is 32.37% shorter than the length of the $\min(\Theta_{\max})$ trajectory. The trajectory obtained with the APF method is the longest. This trajectory is 2.78 times longer than the $\min(\mathrm{L})$ trajectory.

The $\min(\Theta_{\max})$ trajectory allowed to reduce the maximum value of the Euler angles describing the satellite's attitude by 33.46% compared to the straight-line trajectory, by 70.63% compared to the APF trajectory, and by 18.24% compared to the $\min(\mathrm{L})$ trajectory. Thus, the $\min(\Theta_{\max})$ trajectory results in lower disturbances of the chaser's attitude than the three other trajectories. It should be noted that the observed changes in the satellite attitude result not only from the reaction forces and torques induced by the manipulator's motion but also from the initial angular velocity of the chaser. However, the algorithm minimizes attitude changes regardless of their cause. The two variants of the objective function, given in Eqs. (44) and (45), allows us to choose whether we want the smallest possible changes in the satellite's attitude during the maneuver, but at the cost of a longer trajectory, or whether we want the shortest possible trajectory. It is also possible to use an objective function that combines Eqs. (44) and (45) with specific weights, allowing a compromise between minimizing attitude changes and minimizing trajectory length.

The solutions obtained using the proposed method do not violate the constraints defined in Eq. (43). The issue of obstacle avoidance is particularly interesting. Both optimal trajectories are collision-free; thus, $R_{obst}(\boldsymbol{\xi}) = 0$. Figures 2 and 6 show that the minimum-length trajectory results in the end-effector moving along the spherical surface of the obstacle for a certain part of the trajectory. The APF trajectory also allows avoidance of collisions, but results in the highest disturbances of the chaser's attitude. The first phase of this trajectory is very similar to the straight-line trajectory, as the end-effector is attracted towards the desired pose along the shortest line. However, when the end-effector approach the surface of the obstacle, the repulsive force repels the end-effector and it moves away from this obstacle. As evident from Fig. 6, in case of the APF trajectory, the manipulator does not get as close to the surface of the obstacle, as in case of two optimal trajectories. During execution of the straight-line trajectory, links of the manipulator penetrate one of the obstacles (negative distance appearing in Fig. 6), which would result in a collision. Thus, the straight-line trajectory is infeasible for the considered scenario.

5.2. Limitations and future work.

One of the main drawbacks of the presented approach is the lack of guarantee that the global minimum of the objective function has been found, as the optimization algorithm may converge to a local minimum. This drawback is common to all optimal trajectory planning methods developed for free-floating manipulators [22]. However, in the considered scenario, we are primarily interested in finding a solution to the optimization problem that satisfies all constraints, while finding the trajectory that ensures the smallest possible value of the objective function is less important.

Unfortunately, even when a solution exists for a given optimization problem, the interior-point algorithm employed in the proposed method does not guarantee that it will be found. To obtain the results presented in Section 4, the optimization algorithm was initialized with $\boldsymbol{\xi} = \mathbf{0}_{18\times1}$, which is a natural first choice since it results in a straight-line end-effector trajectory. If the algorithm fails to converge to a feasible solution with this initial guess, an alternative initial value of $\boldsymbol{\xi}$ should be used.

The parameterization of the end-effector trajectory in the Cartesian space, while convenient for the considered case in which the chaser has a non-zero initial velocity, presents certain challenges. Specifically, for most values of parameters defining the shape of the trajectory, the trajectory will bring the end-effector outside the manipulator's workspace. One possible solution is to parameterize the trajectory using a sine function with a polynomial argument, which would naturally constrain the area in which the end-effector can be located, regardless of the values of the polynomial coefficients.

Another limitation arises from the fact that the problem of manipulator's dynamic singularities is not addressed. In some scenarios the motion of the end-effector along a planned trajectory in the Cartesian space could cause the manipulator to enter a singular configuration, resulting from the inversion of the $\mathbf{J}_D$ matrix in Eq. (31). Since the WMS-1 Lemur manipulator considered in our study has 7 DoF, it is possible to exploit the manipulator's redundancy and apply a null-space approach to avoid singularities during end-effector motion along the planned trajectory. In such an approach, the desired joint velocities are computed as the sum of the velocities resulting from Eq. (31) and a null-space joint velocity. The null-space velocity is defined as the product of the gradient of a selected

cost function (in this case, a measure of manipulator dexterity in a given configuration) and the orthogonal projection matrix onto the null-space of $\mathbf{J}_D$. This approach was implemented in the Motion Controller developed for the TITAN manipulator [65]. Incorporating this method into the proposed trajectory planning framework appears straightforward. Although different motion in the joint space would result in a different motion of manipulator's links through the Cartesian space, collision avoidance would still be ensured by the penalty function $R_{obst}(\boldsymbol{\xi})$. An alternative approach to addressing the problem of manipulator singularities is to include a term related to the manipulator's dexterity in the objective function $J(\boldsymbol{\xi})$, as proposed in [66]. This allows the trajectory planning algorithm to generate an end-effector Cartesian trajectory that maximizes manipulator dexterity, effectively ensuring that the manipulator remains away from dynamic singularities.

Another noteworthy simplifying assumption that could be dropped in the future is the assumption that obstacles are stationary in Π_{ine}. As explained in the Introduction, ground-based observations indicate that a number of space debris objects exhibit non-zero angular velocity [15, 18]. It may not be feasible to completely stop the rotational motion of such an object using the plume impingement method. To perform capture, the end-effector must achieve zero velocity relative to the selected grasping fixture on the target satellite. Even in case of a rotating object, this can be accomplished using the proposed approach, as any desired final end-effector velocity can be specified. However, non-zero angular velocity of the target would result in non-stationary (dynamic) obstacles with respect to Π_{ine}, necessitating modifications to the proposed approach. This is an interesting direction for further research, as in almost all collision-free trajectory planning methods applicable to a free-floating manipulator, it is assumed that obstacles are stationary [22].

Optimal trajectory planning methods generally entail high computational costs, which could limit their practical application in future space missions. The computational time of the proposed method has not yet been analyzed, as the algorithm is implemented only in Matlab, not in a low-level programming language such as C, and the code has not been optimized. As noted in [67], for highly complex trajectory planning algorithms, one possible approach is to compute the trajectory on Earth and transmit it to the chaser before executing the capture operation. However, this strategy may be infeasible when the chaser has a non-zero initial velocity relative to the target, as the available time for planning and executing manipulator motion is very limited. An alternative, proposed in [68], is to restrict on-board computations to interpolation and selection from a database of optimal trajectories precomputed on Earth.

In future work, we plan to conduct a systematic study of the performance of the proposed trajectory planning method. The analysis will be carried out for several scenarios that differ in the initial conditions, the desired end-effector pose, as well as the number, size, and position of obstacles. The influence of the initial guess on the algorithm's ability to find a solution and its convergence speed will be investigated. The goal of this analysis is to provide a comprehensive characterization of the algorithm's practical reliability and to assess the impact of various parameters on its success rate.

6. CONCLUSIONS

Optimal trajectory planning methods for space manipulators described in the literature often assume that the chaser is either fully controlled during the capture operation or in a free-floating state with zero linear and angular momentum. However, when considering a chaser that is not controlled during the manipulator's motion and is therefore in a free-floating state, its initial velocity at the beginning of the capture operation may not be zero. This is due to the limited accuracy of its control system, which relies on thrusters during the approach phase. Furthermore, in a tangent capture scenario, the chaser's non-zero linear velocity is intentionally set. This paper presents an optimal trajectory planning method for a free-floating space manipulator with constant, non-zero linear and angular momentum, that can take into account the non-zero initial velocity of the chaser. The method enables trajectory planning for the end-effector in the Cartesian space, from an initial pose determined by the satellite-manipulator system's initial configuration to a desired final pose. Additionally, the initial and final velocities of the end-effector can be specified. The approach considers joint position limits and ensures collision avoidance between the manipulator's links and stationary spherical obstacles. The trajectory can be optimized either to minimize its length in the joint space or to reduce the attitude changes of the chaser. The proposed method was successfully validated through numerical simulations conducted using parameters of the prototype of the 7-DoF WMS 1 Lemur space manipulator. Three spherical obstacles in the manipulator's workspace were considered, and trajectories obtained with the proposed approach were compared to two non-optimal trajectories: a straight-line trajectory and a collision-free trajectory obtained with the APF method. Presented results demonstrate that trajectory planning based on optimization methods can be effectively applied to satellite-manipulator systems with non-zero initial velocity at the start of the maneuver. This approach could prove valuable in future ADR and IOS missions.

ACKNOWLEDGEMENTS

This work was supported in part by the Polish National Science Centre project no. 2022/47/D/ST7/02644. The author would like to thank his colleague from Centrum Badań Kosmicznych Polskiej Akademii Nauk (CBK PAN), Dr. Fatina Liliana Basmadji, for her helpful comments and suggestions.

REFERENCES

[1] J. -C. Liou, N. L. Johnson, and N. M. Hill, "Controlling the growth of future LEO debris populations with active debris removal," *Acta Astronaut.*, vol. 66, no. 5-6, pp. 648-653, 2010, doi: 10.1016/j.actaastro.2009.08.005.

[2] M. Shan, J. Guo, and E. Gill, "Review and comparison of active space debris capturing and removal methods," *Prog. Aerosp. Sci.*, vol. 80, pp. 18-32, 2016, doi: 10.1016/j.paerosci.2015.11.001.

[3] W. Zhang, F. Li, J. Li, and Q. Cheng, "Review of on-orbit robotic arm active debris capture removal methods," *Aerospace*, vol. 10, p. 13, 2022, doi: 10.3390/aerospace10010013.

[4] C. G. Henshaw, S. Glassner, B. Naasz, and B. Roberts, "Grappling spacecraft," *Annu. Rev. Control Robot. Auton. Syst.*, vol. 5, no. 1, pp. 137-159, 2022, doi: 10.1146/annurev-control-042920-011106.

[5] S. Estable *et al.*, "Capturing and deorbiting Envisat with an Airbus Spacetug. Results from the ESA e.Deorbit consolidation phase study," *J. Space Saf. Eng.*, vol. 7, no. 1, pp. 52-66, 2020, doi: 10.1016/j.jsse.2020.01.003.

[6] A. Flores-Abad, O. Ma, K. Pham, and S. Ulrich, "A review of space robotics technologies for on-orbit servicing," *Prog. Aerosp. Sci.*, vol. 68, pp. 1-26, 2014, doi: 10.1016/j.paerosci.2014.03.002.

[7] M. Alizadeh and Z. H. Zhu, "A comprehensive survey of space robotic manipulators for on-orbit servicing," *Front. Robot. AI*, vol. 11, p. 1470950, 2024, doi: 10.3389/frobt.2024.1470950.

[8] Y. Xu, "The measure of dynamic coupling of space robot systems," in *Proc. IEEE International Conference on Robotics and Automation (ICRA)*, Atlanta, GA, USA, 1993, pp. 615-620, doi: 10.1109/ROBOT.1993.291837.

[9] R. Rank, Q. Mühlbauer, W. Naumann, and K. Landzettel, "The DEOS Automation and Robotics Payload," in *Proc. 11th ESA Workshop on Advanced Space Technologies for Robotics and Automation (ASTRA)*, ESTEC, Noodwijk, The Netherlands, 2011.

[10] N. Inaba and M. Oda, "Autonomous satellite capture by a space robot: world first on-orbit experiment on a Japanese robot satellite ETS-VII," in *Proc. IEEE International Conference on Robotics and Automation (ICRA)*, San Francisco, CA, USA, 2000, pp. 1169-1174, doi: 10.1109/ROBOT.2000.844757.

[11] A. Ogilvie, J. Allport, M. Hannah, and J. Lymer, "Autonomous robotic operations for on-orbit satellite servicing," *Proceedings of SPIE 6958, Sensors and Systems for Space Applications II*, p. 695809, 2008. https://doi.org/10.1117/12.784081.

[12] S. Dubowsky and E. Papadopoulos, "The kinematics, dynamics, and control of free-flying and free-floating space robotic systems," *IEEE Trans. Robot. Autom.*, vol. 9, no. 5, pp. 531-543, 1993, doi: 10.1109/70.258046.

[13] J. Ratajczak and K. Tchoń, "Normal forms and singularities of non-holonomic robotic systems: A study of free-floating space robots," *Syst. Control Lett.*, vol. 138, p. 104661, 2020, doi: 10.1016/j.sysconle.2020.104661.

[14] W. Domski and A. Mazur, "Input-output decoupling for a 3D free-floating satellite with a 3R manipulator with state and input disturbances," *Bull. Polish Acad. Sci. Tech. Sci.*, vol. 67, no. 6, pp. 1031-1039, 2019, doi: 10.24425/bpasts.2019.130885.

[15] A. Smagło *et al.*, "Measurements to space debris in 2016–2020 by laser sensor at Borowiec Poland," *Artif. Satell.*, vol. 56, no. 4, pp. 119-134, 2021, doi: 10.2478/arsa-2001-0009.

[16] K. Seweryn and J. Z. Sasiadek, "Satellite angular motion classification for active on-orbit debris removal using robots," *Aircr. Eng. Aerosp. Tech.*, vol. 91, no. 2, pp. 317–332, 2019, doi:10.1108/AEAT-01-2018-0049.

[17] N. O. Gómez and S. J. Walker, "Earth's gravity gradient and eddy currents effects on the rotational dynamics of space debris objects: Envisat case study," *Adv. Space Res.*, vol. 56, no. 3, pp. 494-508, 2015, doi: 10.1016/j.asr.2014.12.031.

[18] J-N. Pittet, J. Šilha, and T. Schildknecht, "Spin motion determination of the Envisat satellite through laser ranging measurements from a single pass measured by a single station," *Adv. Space Res.*, vol. 61, no. 4, pp. 1121–1131, 2018, doi:10.1016/j.asr.2017.11.035.

[19] T. Peters and D. E. Olmos, "Applicability of COBRA concept to detumbling space debris objects," in *Proc. 6th International Conference on Astrodynamics Tools and Techniques (ICATT)*, Darmstadt, Germany, 2016.

[20] Y. Nakajima, H. Tani, S. Mitani, and T. Yamamoto, "Efficiency improving guidance for detumbling of space debris using thruster plume impingement," in *Proc. 2020 IEEE Aerospace Conference*, Big Sky, MT, USA, 2020, doi: 10.1109/AERO47225.2020.9172511.

[21] J. Ratajczak, "Nonholonomic motion planning with special restrictions on the end and via points of the control function," *Bull. Polish Acad. Sci. Tech. Sci.*, vol. 73, no. 2, p. e153427, 2025, doi: 10.24425/bpasts.2025.153427.

[22] T. Rybus, "Obstacle avoidance in space robotics: Review of major challenges and proposed solutions," *Prog. Aerosp. Sci.*, vol. 101, pp. 31-48, 2018, doi: 10.1016/j.paerosci.2018.07.001.

[23] X. Gao, Q. Jia, H. Sun, and G. Chen, "Research on path planning for 7-DOF space manipulator to avoid obstacle based on A* algorithm," *Sens. Lett.*, vol. 9, no. 4, pp. 1515-1519, 2011, doi: 10.1166/sl.2011.1665.

[24] J. R. Benevides and V. Grassi, "Autonomous path planning of free-floating manipulators using RRT-based algorithms," in *Proc. 12th IEEE Latin American Robotics Symposium and 3rd Brazilian Symposium on Robotics (LARS-SBR)*, Uberlandia, Minas Gerais, Brazil, 2015, pp. 139-144, doi: 10.1109/LARS-SBR.2015.47.

[25] T. Rybus, J. Prokopczuk, M. Wojtunik, K. Aleksiejuk, and J. Musiał, "Application of bidirectional rapidly exploring random trees (BiRRT) algorithm for collision-free trajectory planning of free-floating space manipulator," *Robotica*, vol. 40, no. 12, pp. 4326-4357, 2022, doi: 10.1017/S0263574722000935.

[26] T. Rybus, "The Obstacle Vector Field (OVF) method for collision-free trajectory planning of free-floating space manipulator," *Bull. Polish Acad. Sci. Tech. Sci.*, vol. 70, no. 2, p. e140691, 2022, doi: 10.24425/bpasts.2022.140691.

[27] J. Lu and H. Yang, "Trajectory planning of satellite base attitude disturbance optimization for space robot," in *Proc. 3rd IEEE International Conference on Control and Robots (ICCR)*, Tokyo, Japan, 2020, pp. 85-89, doi: 10.1109/ICCR51572.2020.9344311.

[28] C. Toglia, M. Sabatini, P. Gasbarri, and G. B. Palmerini, "Optimal target grasping of a flexible space manipulator for a class of objectives," *Acta Astronaut.*, vol. 68, no. 7-8, pp. 1031-1041, 2011, doi: 10.1016/j.actaastro.2010.09.013.

[29] T. Rybus, M. Wojtunik, and F. L. Basmadji, "Optimal collision-free path planning of a free-floating space robot using spline-based trajectories," *Acta Astronaut.*, vol. 190, pp. 395-408, 2022, doi: 10.1016/j.actaastro.2021.10.012.

[30] O. P. Agrawal and Y. Xu, "On the global optimum path planning for redundant space manipulators," *IEEE Trans. Syst. Man. Cybern.*, vol. 24, no. 9, pp. 1306-1316, 1994, doi: 10.1109/21.310507.

[31] K. Seweryn and M. Banaszkiewicz, "Optimization of the trajectory of a general free-flying manipulator during the rendezvous maneuver," in *Proc. AIAA Guidance, Navigation and Control Conference and Exhibit (AIAA-GNC)*, Honolulu, Hawaii, 2008, doi: 10.2514/6.2008-7273.

[32] X. P. Wei, J. X. Zhang, D. S. Zhou, and Q. Zhang, "Optimal path planning for minimizing base disturbance of space robot," *Int. J. Adv. Robot. Syst.*, vol. 13, no. 2, 2016, doi: 10.5772/62126.

[33] X. Liu, H. Baoyin, and X. Ma, "Optimal path planning of redundant free-floating revolute-jointed space manipulators with seven links," *Multibody Syst. Dyn.*, vol. 29, pp. 41-56, 2013, doi: 10.1007/s11044-012-9323-x.

[34] Z. Chen and W. Zhou, "Path Planning for a Space-Based Manipulator System Based on Quantum Genetic Algorithm," *J. Robot.*, vol. 2017, p. 3207950, 2017, doi: 10.1155/2017/3207950.

[35] D. Qiao, "Motion planning optimization of trajectory path of space manipulators," *Int. J. Metrol. Qual. Eng.*, vol. 10, p. 11, 2019, doi: 10.1051/ijmqe/2019011.

[36] R. Jin, P. Rocco, and Y. Geng, "Cartesian trajectory planning of space robots using a multi-objective optimization," *Aerosp. Sci. Technol.*, vol. 108, p. 106360, 2021, doi: /10.1016/j.ast.2020.106360.

[37] F. Cavenago, A. M. Giordano, and M. Massari, "Contact force observer for space robots," in *Proc. 58th IEEE Conference on Decision and Control (CDC)*, Nice, France, 2019, pp. 2528-2535, doi: 10.1109/CDC40024.2019.9029285.

[38] F. Han, H. Wu, J. Hou, Z. Wang, S. Lu, and Y. Sun, "The 6-DOF synchronized sliding-mode control for approaching to the slowly rotating satellite," in *Proc. 34th IEEE Chinese Control Conference (CCC)*, Hangzhou, China, 2015, pp. 3269-3274, doi: 10.1109/ChiCC.2015.7260144.

[39] L. Fan and H. Huang, "Coordinative coupled attitude and orbit control for satellite formation with multiple uncertainties and actuator saturation," *Acta Astronaut.*, vol. 181, pp. 325-335, 2021, doi: 10.1016/j.actaastro.2021.01.039.

[40] K. Seweryn, F. L. Basmadji, T. Rybus, "Tangent capture of an uncontrolled target satellite by space robot: simulation studies," in *Proc. 2020 AIAA SciTech Forum and Exposition*, Orlando, Florida, USA, 2020, doi: 10.2514/6.2020-1602.

[41] K. Seweryn, F. L. Basmadji, T. Rybus, "Space robot performance during tangent capture of an uncontrolled target satellite," *Astronaut. Sci.*, vol. 69, pp. 1017-1047, 2022, doi: 10.1007/s40295-022-00330-2.

[42] T. Rybus, K. Seweryn, J. Z. Sąsiadek, "Trajectory optimization of space manipulator with non-zero angular momentum during orbital capture maneuver," in *Proc. AIAA Guidance, Navigation, and Control*

Conference (AIAA-GNC), San Diego, CA, USA, 2016, doi: 10.2514/6.2016-0885.
[43] A. Seddaoui and C. M. Saaj, "Collision-free optimal trajectory generation for a space robot using genetic algorithm," *Acta Astronaut.*, vol. 179, pp. 311-321, 2021, doi: 10.1016/j.actaastro.2020.11.001.
[44] W. Zhang and H. Wen, "Motion planning of a free-flying space robot system under end effector task constraints," *Acta Astronaut.*, vol. 199, pp. 195-205, 2022, doi: 10.1016/j.actaastro.2022.07.005
[45] O. Zhang *et al.*, "Trajectory optimization and tracking control of free-flying space robots for capturing non-cooperative tumbling objects," *Aerosp. Sci. Technol.*, vol. 143, p. 108718, 2023, doi: 10.1016/j.ast.2023.108718.
[46] K. Seweryn *et al.*, "The prototype of space manipulator WMS LEMUR dedicated to capture tumbling satellites in on-orbit environment," in *Proc. 11th International Workshop on Robot Motion and Control (RoMoCo)*, Wąsowo, Poland, 2017, pp. 15-22, doi: 10.1109/RoMoCo.2017.8003887.
[47] Y. Umetani and K. Yoshida, "Continuous path control of space manipulators mounted on OMV," *Acta Astronaut.*, vol. 15, no. 12, pp. 981-986, 1987, doi: 10.1016/0094-5765(87)90022-1.
[48] M. Wojtunik, "Stable adaptive control system dedicated to space manipulator with mechatronic constraints," Ph.D. thesis, Centrum Badań Kosmicznych Polskiej Akademii Nauk, Poland, 2025.
[49] H. Schaub and J. L. Junkins. *Analytical mechanics of Space Systems*. Reston, VA: American Institute of Aeronautics and Astronautics, 2018.
[50] L. Meirovitch. *Methods of Analytical Dynamics*. New York, NY: McGraw Hill, 1970.
[51] F. L. Basmadji, K. Seweryn, and J. Z. Sasiadek, "Space robot motion planning in the presence of nonconserved linear and angular momenta," *Multibody Syst. Dyn.*, vol. 50, pp. 71-96, 2020, doi: 10.1007/s11044-020-09753-x.
[52] K. Yoshida and Y. Umetani, "Control of Space Manipulators with Generalized Jacobian Matrix," in *Space Robotics: Dynamics and Control*, Y. Xu and T. Kanade, Eds. New York, NY: Springer, 1993, pp. 165–204, doi: 10.1007/978-1-4615-3588-1_7.
[53] P. Palma, T. Rybus, and K. Seweryn, "Application of Impedance Control of the Free Floating Space Manipulator for Removal of Space Debris," *Pomiary Automatyka Robotyka*, vol. 27, no. 3, pp. 95-106, 2023, doi: 10.14313/PAR_249/95.
[54] K. Yoshida, "Experimental study on the dynamics and control of a space robot with experimental free-floating robot satellite," *Adv. Robot.*, vol. 9, no. 6, pp. 583-602, 1994, doi: 10.1163/156855395X00319.
[55] A. Ben-Israel and T. N. Greville. *Generalized inverses: theory and applications*, 2nd ed. New York, NY. Springer-Verlag, 2003.
[56] E. Papadopoulos and S. Dubowsky, "Dynamic singularities in free-floating space manipulators," *J. Dyn. Sys. Meas. Control*, vol. 115, no. 1, pp. 44-52, 1993, doi: 10.1115/1.2897406.
[57] Q. Jia, Y. Liu, G. Chen, and H. Sun, "Maximum load path planning for space manipulator in point-to-point task," in *Proc. 8th IEEE Conference on Industrial Electronics and Applications (ICIEA)*, Melbourne, Australia, 2013, pp. 988-993, doi: 10.1109/ICIEA.2013.6566511.
[58] R. Mukherjee and Y. Nakamura, "Nonholonomic redundancy of space robots and its utilization via hierarchical liapunov functions," in *Proc. American Control Conference (ACC)*, Boston, MA, USA, 1991, pp. 1491-1496, doi: 10.23919/ACC.1991.4791630.
[59] T. Rybus and K. Seweryn, "Trajectory planning and simulations of the manipulator mounted on a free-floating satellite," in *Aerospace Robotics, GeoPlanet: Earth and Planetary Sciences*, J. Sąsiadek, Ed. Berlin, Heidelberg: Springer, 2013, pp. 61-73, doi: 10.1007/978-3-642-34020-8_6.
[60] O. Khatib, "Real-Time Obstacle Avoidance for Manipulators and Mobile Robots," *Int. J. Rob. Res.*, vol. 5, no. 1, pp. 396–404, 1986, doi: 10.1177/027836498600500106.
[61] C. C. Lin and J. H. Chuang, "Potential-based path planning for robot manipulators in 3-D workspace," in *Proc. IEEE International Conference on Robotics and Automation (ICRA)*, Taipei, Taiwan, 2003, pp. 3353-3358, doi: 10.1109/ROBOT.2003.1242108.
[62] T. Rybus and K. Seweryn, "Zastosowanie metody sztucznych pól potencjału do planowania trajektorii manipulatora satelitarnego," [in polish: "Application of the artificial potential field method for trajectory planning of space manipulator"] in *Postępy Robotyki, Prace Naukowe Politechniki Warszawskiej: Elektronika*, vol. 196, K. Tchoń and C. Zieliński, Eds. Oficyna Wydawnicza Politechniki Warszawskiej, 2018, pp. 61-74 .
[63] K. Seweryn *et al.*, "The laboratory model of the manipulator arm (WMS1 LEMUR) dedicated for on-orbit operation," in *Proc. 12th International Symposium on Artificial Intelligence, Robotics and Automation in Space (i-SAIRAS)*, Saint-Hubert, Quebec, Canada, 2014.
[64] J. Schulman *et al.*, "Finding locally optimal, collision-free trajectories with sequential convex optimization," in *Proc. Robotics: Science and Systems IX*, Berlin, Germany, 2013, doi: 10.15607/RSS.2013.IX.031.
[65] T. Rybus *et al.*, "Motion Controller for the TITAN robotic manipulator dedicated for on-orbit servicing operations," in *Proc. 17th Symposium on Advanced Space Technologies in Robotics and Automation (ASTRA)*, Leiden, The Netherlands, 2023.
[66] X. Lu and Y. Jia, "Trajectory planning of free-floating space manipulators with spacecraft attitude stabilization and manipulability optimization," *IEEE Trans. Syst. Man Cybern. Syst.*, vol. 51, no. 12, pp. 7346-7362, 2020, doi: 10.1109/TSMC.2020.2966859.
[67] T. Rybus, K. Seweryn, and J. Z. Sąsiadek, "Application of trajectory optimization method for a space manipulator with four degrees of freedom," in *Proc. 13th International Conference on Informatics in Control, Automation and Robotics (ICINCO)*, Lisbon, Portugal, 2016, pp. 92-101, doi:10.5220/0005981000920101
[68] R. Lampariello and G. Hirzinger, "Generating feasible trajectories for autonomous on-orbit grasping of spinning debris in a useful time," in *Proc. IEEE/RSJ International Conference on Intelligent Robots and Systems*, Tokyo, Japan, 2013, pp. 5652-5659, doi:10.1109/IROS.2013.6697175.